α-Synuclein pathology and mitochondrial dysfunction

van Zomeren, Koen Cornelis

Chapter 3

Using metabolic preference for the highly efficient generation of pure neuronal populations from human induced pluripotent stem cells

Neuronal selection using a lactate switch

Koen C. van Zomeren, Susanne M. Kooistra, Hilmar R.J. van Weering, Rob Bakels, Erik Boddeke and Sjef Copray

Department of Neuroscience, University Medical Centre Groningen, University of Groningen, Groningen, The Netherlands

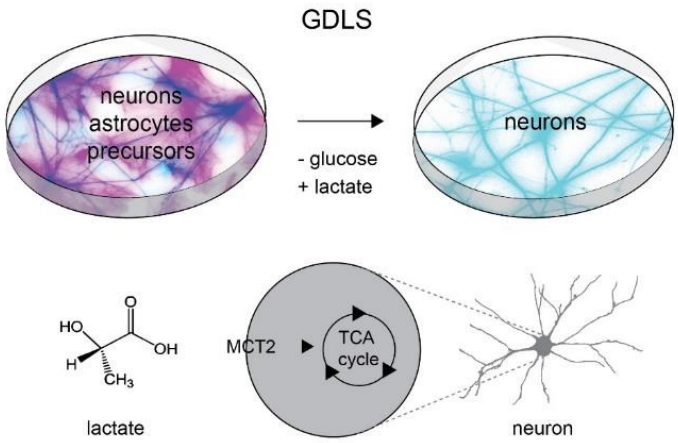

Graphical abstract

Glucose deprivation and lactate supplementation (GDLS) treatment of differentiating hiPSCs results in highly pure (>90%) neuronal cultures. Monocarboxylate transporter 2 is required for the selective survival of neurons. GDLS provides a low-cost, robust method for generating pure neuronal cultures.

Submitted

Abstract

Differentiated human induced pluripotent stem cells (hiPSCs) hold great promise as a source for autologous cells for cell replacement therapies and disease modeling. While the initial yield of differentiated cells can be high, cultures are often contaminated with a variety of unwanted cellular phenotypes. Moreover, current methods to obtain pure populations of specific differentiated cell types are laborious, expensive and often difficult to reproduce. We present an efficient method to purify hiPSC-derived neuronal cultures utilizing their metabolic capacity through supplying selective metabolic substrates based on glucose deprivation and lactate supplementation (GDLS). hiPSC-derived neurons that were purified by GLDS show electrophysiological activity, similar to unpurified hiPSC-derived neurons, and can be cultured for a prolonged duration. The GDLS purification procedure is equally effective for patient and control iPSC-derived neurons. This brief, simple and cost-effective method to obtain pure hiPSC-derived neuronal cultures creates new opportunities for hiPSC-associated neuronal disease modeling.

Introduction

Human induced pluripotent stem cells (hiPSCs) offer an advanced tool for disease modelling, drug screening and cell replacement therapies (1, 2). Unlimited self-renewal and the potential to differentiate into cells of all three germ layers provide an unprecedented source for otherwise unobtainable autologous cells that can be used for disease modeling or transplantation purposes. However, hiPSC-based generation of specific cellular populations with high efficiency and purity has proven to be a major challenge for a number of lineages, including the dopaminergic neuronal lineage (3, 4).

hiPSCs are frequently used to generate neuronal subtypes to model neurodegenerative disorders and are currently considered for cell transplantation as regenerative therapy. Parkinson's disease (PD) is one of the most obvious candidates for such a cell replacement therapy, since early neuronal pathology is largely confined to the nigrostriatal pathway, and characterized by loss of dopaminergic (DA) neurons in the substantia nigra pars compacta (5). Moreover, ample experience with cell transplantation approaches in PD patients using abortion-derived fetal DA neurons has already demonstrated its feasibility and therapeutic efficacy in the 80's and 90's (6).

A major bottleneck in stem cell-based replacement therapy is the impurity of the DA cell graft. Apart from contaminating, undifferentiated and possibly teratogenic iPSCs, other neuronal and in particular non-neuronal cell types may still be present, interfering with therapeutic outcome. Current strategies to eliminate or decrease unwanted populations of cells include laborious and harmful sorting techniques (7-9), application of mitosis-inhibiting chemicals like mitomycin C (10) or the use of neuronal cells at early time-points (<40 days in vitro (DIV)) (11-13). Harmful elimination and purification steps are considered highly undesirable in current procedures for replacement strategies or disease modeling. Furthermore, use of less mature neuronal cells is questionable given the nature of most late-onset neuronal disorders studied with iPSCs.

Apart from this, estimation of differentiation efficiency at early time points can lead to an overestimation of neuronal content at later time points, since contaminating populations often proliferate.

To improve the outcome of differentiation procedures, we implemented a novel strategy to purify iPSC-derived neuronal populations based on their metabolic properties. Replacing glucose and using lactate as a metabolic substrate effectively annihilates the presence of glial- and neuronal precursor populations, which are glucose-dependent, in neuronal differentiated cell cultures. In addition to presenting an effective tool for neuronal purification, our method also provides further evidence for the brain lactate shuttle hypothesis, originally proposed over 20 years ago (14). This concept has gained renewed attention through the first evidence for this shuttle in vivo (15). In the central nervous system, astrocytes and oligodendrocytes produce lactate, which is exported via the low affinity monocarboxylate transporter (MCT) 4 and/or MCT1, to be taken up by the high affinity MCT2 transporter expressed by neurons (16). The neuronal lactate shuttle hypothesis states that neurons can take up lactate in case of high energy demand, such as during stroke and even brain development (15, 17-19). In contrast, the primary metabolic pathways in pluripotent stem cells are dependent on glucose and glycolysis (20).

We hypothesized that lactate shuttling is active in hiPSCs-derived neurons and can be exploited in combination with glucose deprivation to selectively sustain neuronal populations. In contrast, progenitor, glial and undifferentiated counterparts are glucose-dependent. In this study, we present a method to derive functional neuronal populations from iPSCs with high purity by combining existing iPSC differentiation protocols with glucose deprivation and lactate supplementation (GDLS).

GDLS-treated neurons in our study show mature action potentials, spontaneous neuronal activity and express mature neuronal markers.

Moreover, we have cultured these neurons for prolonged periods, up to 90 DIV, which is a requirement for proper disease modelling.

Materials and methods

Cell culture

Fibroblast cell lines from Parkinson patients were obtained from Corriel biorepository (ND27760, ND40996). Healthy donor fibroblast lines were acquired from the UMCG Department of Dermatology. Generation of iPSCs was done following the protocol and using episomal vectors from Okita et al. (2011). Briefly, to generate iPSCs, one million fibroblasts were nucleofected with 0.85 µg pCXLE-hMLN, 0.85 µg pCXLE-hOCT3/4 and 1.3 µg pCXLE-hSK (Addgene #27079, #27076, #27078). Clones were checked for expression of pluripotency factors (OCT3/4, SOX2, KLF4, TRA1-60, TRA-1-81, live alkaline phosphatase) and karyotype was assessed using metaphase spreads. Differentiation potential was assessed by spontaneous embryoid body (EB) differentiation, using antibodies for ectoderm (TUJ1), endoderm (GATA4) and mesoderm (DESMIN). H9 ESCs were used in collaboration with the Department of Experimental Cardiology, UMCG. Cells were maintained on Geltrex® coated plates in Essential 8™ medium (Thermo Fisher), and passaged weekly using ReLeSR™ (Stemcell Technologies). All cells were used for experiments between passage 20 and 50, and kept in a humidified incubator at 37°C with 5%CO_2.

Neuronal differentiation

For differentiation, a slightly adapted protocol from Kriks et al. was followed (21). Briefly, cells were grown to 70% confluency, and medium was changed to 50% KSR and 50% DMEM/F12. Over the course of 7 days, medium was changed to DMEM/F12 supplemented with N1 (Sigma). The following small molecules and proteins were added; 10 µM SB-431542 (Stemcell Technologies) from day 1-5, 100nM LDN-193189

(Stemcell Techologies) from day 1-11, 3 μM Purmorphamine (Stemcell Techologies) from day 3-7, 500 nM Smoothened agonist from day 3-7, 100 ng/ml SHH (Peprotech) from day 3-8, 50 ng/ml FGF8 (Peprotech) from day 3-8 and 2 μM CHIR99021 (Stemcell Technologies) from day 5-13. Terminal neuronal induction towards a dopaminergic ventral midbrain phenotype was started at day 12 by switching to Neurobasal A™ (NBA) medium supplemented with SM1-Vit.A 50x (Stemcell Techologies), N1 250x (Sigma), BDNF (20 ng/ml, Peprotech), Ascorbic Acid (200 μM, Sigma), GDNF (20 ng/ml, Peprotech), dibutyryl cAMP (0.5 mM, Sigma), DAPT (10 μM, Stemcell Technologies), and TGF-β3 (1 ng/ml, Peprotech) (BAGCDT). Eighteen to twenty days after the start of differentiation cells were dissociated using Accutase (Sigma), strained with a 45μM cell strainer to remove cell debris, and plated on Geltrex® coated tissue culture treated plates at a density of roughly 80.000 cells/cm^2.

For motor neuron differentiation a modified protocol was used (S2A Fig). Cells were grown in similar conditions as described above, with addition of 10 μM SB-431542 (Stemcell Technologies) from day 1-5, 100nM LDN-193189 (Stemcell Techologies) from day 1-11, 3 μM Purmorphamine (Stemcell Techologies) from day 3-7, 500 nM Smoothened agonist from day 3-7, 100 ng/ml SHH (Peprotech) from day 3-8, 10 μM all-trans retinoic acid (RA; Peprotech) from day 5-20 and 2 μM CHIR99021 (Stemcell Technologies) from day 5-13.

Glucose deprivation and lactate supplementation (GDLS)

GDLS was initiated between 26 days and 36 days of differentiation, and was carried out for a period of 4-6 days based on visual inspection of the plate. NBA medium without glucose and sodium pyruvate supplemented with BAGCDT, SM1 50x and N1 250x, was added to the wells and supplemented with sodium DL-lactate (Sigma, L1375) to a final concentration of 5 mM. Cells were inspected daily to assess the GDLS based selection, and media was changed every other day. After cessation

of GDLS treatment, cells were recovered in glucose supplemented (25 mM) NBA and used for subsequent analysis.

Cell imaging

Phase contrast imaging was performed on a Leica AF-6000 microscope, using a 20x objective (PL FLUOTAR 20x/NA 0.4, Dry). Phase contrast images were taken at fixed positions in each well, to prevent biased imaging.

Large-scale tile scan imaging was performed using Tissuegnostics TissueFaxs setup, using a 10x phase contrast Zeiss-objective (Plan-Neofluar 10x/NA 0.3, Dry). Fully automated tile scans were performed in 6-well plates, and stitching was done using TissueFaxs viewer software (v3.5).

Calcium imaging recordings

Cells were replated at 80.000 cells/cm^2 on Geltrex® coated Nunc™ Lab-Tek™ II chamber slides™. Medium was switched to BrainPhys™ medium (Stemcell Technologies) plus growth factors to electrically mature neurons 14 DIV before imaging. Cells were incubated with 0.5 µM Fluo-AM (Thermo Fisher, Cat No. F14217) and placed inside an imaging chamber at 37°C with 5% CO2 and 95% humidity without washing. Calcium imaging movies were recorded using the Deltavision Elite live cell imaging system (GE Healthcare) equipped with PLAPON 60x oil, NA 1.42, WD 0.15 mm (Olympus) and a 15-bit EDGE/sCMOS camera (PCO) with GFP live filter wheel settings. At least 5 movies ranging from 1 min to 2 min intervals were recoded for selected cells, with timeframes ranging from 0.1 s to 0.5 s at 3.2% illumination intensity. Time series analysis was done using ImageJ (1.49s), by plotting y-axis profiles for both whole image analysis and regions of interest (ROIs). Neuronal calcium events were defined as a sharp transient increase in fluorescence intensity (Fluo-4 AM, dF/F >5%, fast rise, slower decay).

Electrophysiological recordings

Selected and non-selected cells were plated on Geltrex® coated coverslips at 45 DIV, and electrically matured in supplemented BrainPhys™ medium. At 60 DIV, coverslips were placed in a measuring chamber attached to an inverted microscope (Axioskop 2 FS, Zeiss) with a 40X water-immersion objective (NA 0.8, W ACHROPLAN). Membrane currents and voltages were measured using an Axopatch 200 B patch clamp amplifier (Molecular Devices) in whole-cell mode. Pipettes were pulled from GC120F-10 borosilicate glass (Harvard Apparatus, Holliston, MA) and filled with a solution containing 140 mM KCl, 10 mM Hepes, 1 mM MgCl2, 10 mM EGTA, 1 mM $CaCl_2$ and 2 mM Na_2ATP (280–290 mOsm, pH 7.4). Bathing solution contained 140 mM NaCl, 4 mM KCl, 1 mM $MgCl_2$, 2 mM $CaCl_2$, 1.2 mM HEPES and 10 mM glucose (mOsm 330, pH 7.4). Membrane currents were recorded at room temperature (20–22°C) with the amplifier in whole cell voltage clamp mode. Recording quality was continuously assessed by monitoring resistance and leak current. Initial pipette resistance was between 4 and 8 MΩ, with series resistance in samples averaging 50 MΩ. Currents were low-pass filtered at 5 kHz and sampled at 10 kHz using a Digidata 1320 AD converter (Molecular Devices). Currents were evoked by a voltage protocol, from -70 mV to +30 mV in 10 mV increments. After measuring membrane currents, the amplifier was switched to current clamp mode. Following measurement of the resting potential, the membrane potential was adjusted to -60 mV using a steady injected current through the patch pipette. Action potentials were evoked by depolarizing current pulses (50 ms duration in order to analyze single spikes, and 500 ms pulses to induce repetitive firing. Voltage clamp step protocols were generated and data were analyzed using Pclamp software (Molecular Devices).

Immunocytochemistry

Neuronal cultures on glass coverslips or 6-well plates were fixed in paraformaldehyde 4% for 15 min at room temperature. Samples were

permeabilized and blocked with PBS containing 0.1% Triton, 1% BSA and 5% normal goat serum for ~60 min at RT. Samples were incubated with primary antibodies overnight at 6°C, then washed 3 times with PBS and incubated with a fluorescent conjugated secondary antibody and Hoechst 33258 (Sigma, 14530). Mowiol® 4-88 (Sigma) was used as mounting medium to attach coverglasses to the coverslip. Samples were stored at 4°C until further analysis.

Fluorescent imaging and analysis

Single fluorescent images were acquired using a Leica AF-6000 fluorescent microscope, using a PL FLUOTAR 20x/NA 0,4, Dry lens. Images were analyzed using the ImageJ cell counter plugin.

Large-scale tile scan imaging was performed using Tissuegnostics TissueFaxs equipment, with a 10x phase contrast Zeiss-objective (Plan-Neofluar 10x/NA 0.3, Dry). Fully automated tile scans were performed in 6-well plates, and stitching was done using TissueFaxs viewer (v3.5) software. Analysis with ImageJ was performed on complete tile scans, assessing the total surface of signal from each fluorophore.

Antibodies

The following primary antibodies were used: Alkaline Phosphatase Live Stain (Thermo Fischer, A14353), βIII-Tubulin (mouse, 1:1000, Abcam, ab7751), DESMIN (mouse, 1:1000, DAKO, M0760), GATA4 (mouse, 1:1000, Santa Cruz Biotechnology, sc25310) Glial fibrillary acidic protein (rabbit, 1:1000, Dako, Z0334), NANOG (rabbit, 1:500, Abcam, ab80892), OCT3/4 (rabbit, 1:500, Santa Cruz Biotechnology, sc-9081), SOX2 (mouse, 1:500, Cell Signaling, #4900S), SSEA4 (mouse, 1:500, Hybridoma Bank, MC-813-70), TRA1-81 (mouse, 1:500, Santa Cruz Biotechnology, sc-21706), Tyrosine hydroxylase (rabbit, Abcam, AB152), Tyrosine hydroxylase (mouse, 1:1000, Immunostar, 22941). The following secondary fluorescently conjugated antibodies were used at 1:500 dilution: Goat anti-mouse Cy3 (Jackson Immuno Research, 115-165-

003), goat-anti-rabbit-DyLight 488 (Thermo Fisher, 35552), donkey anti-mouse-AF488 (Mol Probes, Thermo Fisher, A21202), donkey anti-rabbit Cy3 (Jackson Immuno Research, 711-165-152).

Quantitative Real-Time PCR

Total RNA was extracted with an RNeasy Mini kit (Qiagen) and quantitative RT–PCR reaction was performed using the maxima SYBR Green/ROX master mix (Thermo Scientidic). CDNA was reverse transcribed from 1 µg of RNA using M-MLV Reverse Transcriptase (Thermo-Scientific). Primers were acquired from Biolegio and reactions were run on a Roche Lightcycler® 480 and analyzed with accessory software (v1.5). Expression levels were normalized to endogenous *HMBS* levels, and fold-change in gene expression was calculated using the $2^{\Delta\Delta CT}$ method.

The following primers were used. *FOXA2* (NM-153675, forward; GGAGCAGCTACTATGCAGAG, reverse; CTCATGTACGTGTTCATGCC), *GIRK2* (NM_002240, forward; GCCAGGAAAAGCACAAAGAA, reverse; CTTTCGACGTCCTGATCCAT), *HMBS* (NM-001024382.1, forward; TGCCAGAGAAGAGTGTGGT, reverse; CCGAATACTCCTGAACTCC), *LDHA* (NM_005566, forward; GGCCTGTGCCATCAGTATCT, reverse; GGAGATCCATCATCTCTCCC), *LMX1A* (NM-177398, forward; GACTACGAGAAGCTGTTTGCT, reverse; GCAGCTCAGGTGGTATACAC), *MCT2* (NM_004731, forward; CAACACCATTCCAAGACAGC, reverse; TGGCTGTTATGTACGCAGGA), *NURR1* (NM-006168, forward; ATTAGCATACAGGTCCAACCC, reverse; ACAATGGAATCAATCCATTCCC), *SNCA* (NM-000345, forward; AAGAGGGTGTTCTCTATGTAGGC, reverse; GCTCCTCCAACATTTGTCACTT), *SOX2* (NM-003106, forward; CACAACTCGGAGATCAGCAA, reverse; CGGGGCCGGTATTTATAATC), *TH* (NM-199292, forward; GAGATCGCCTTCCAGTACAG, reverse; TGGTGTAGACCTCCTTCCAG), *TUJ1* (NM_00107.4, forward; GGCCTCTTCTCACAAGTACG, reverse; GAAGAGATGTCCAAAGGCCC).

Statistical analysis

All statistical tests were performed using Sigmaplot 13.0. Statistical significance was determined with the nonparametric Mann–Whitney *U* test. A p value < 0.05 was considered significant. Data are presented as minimum to maximum whisker box plots or dot plots.

Results

GDLS is compatible with neuronal differentiation protocols and results in highly pure neuronal cultures

To explore the validity of the hypothesis that lactate can selectively sustain neurons in vitro, we applied GDLS to a dual SMAD inhibition based protocol (22) combined with a protocol inducing dopaminergic patterning *(21)*. While GDLS works on all dual SMAD inhibition based protocols, we have chosen to implement our procedure on the dopaminergic differentiation protocol, since this enables us to determine the relative sensitivity of a neuronal subtype (i.e. DA neurons) to GDLS.

In dual SMAD inhibition based DA differentiation, cells are first differentiated to neural floor plate precursor cells, followed by more terminal neuronal induction towards a dopaminergic ventral midbrain phenotype (Fig 1A). The maturation of functional neurons capable of generating action potentials can take up to 60 DIV, and markers for mature dopaminergic cells such as GIRK2 appear between 60 and 90 DIV.

To implement GDLS, we first passaged differentiated cell cultures after 18 DIV. Subsequently, between 26 DIV and 36 DIV, cells were fully deprived of glucose and simultaneously supplied with lactate (5mM) for 4-6 days. Medium was changed back to glucose-containing (25mM) medium based on visual inspection of the absence of contaminating cells in the culture. Finally, cells were allowed to recover for a minimum of six days in glucose containing medium before passaging or subsequent analysis.

Gross morphological analysis indicates that GDLS treatment of differentiated hiPSC cultures results in more uniform cell cultures, where the majority of cells have a neuronal morphology with small soma and large processes (Fig 1B). The advantageous effect of GDLS on the purity of the culture is independent of disease background, as both control and familial PD patient iPSC lines showed a similar response to GDLS. Images represent randomly selected excerpts from large tile scan stitches (>2.5 cm^2 surface) taken at 45 DIV. PD patient lines used carry mutations in the *SNCA* gene leading to familial PD. PD4 contains a triplication of the *SNCA* genomic region and PD1 contains the *SNCA* gene G209A mutation causing an A53T mutation in the α-synuclein protein.

Figure 1C illustrates immunofluorescent analysis of βIII tubulin (TUJ1, green), tyrosine hydroxylase (TH, red) and nuclei (Hoechst, blue) of GDLS-treated and non-treated cultures of the PD4 iPSC line at 60DIV (bars 50 μm). In comparison to previous protocols (3, 10, 11, 23, 24), GDLS almost annihilates the presence of non-neuronal cell types and drastically increases the relative proportion of neurons (34.2% of TUJ1 positive cells in control against 93.3% in GDLS-treated, Fig 1C, D). Consequently, the fraction of dopaminergic neurons within the total cell population is increased (8.3% vs. 27.3% TH positive cells). However, within the population of neuronal cells, the relative contribution of dopaminergic neurons is maintained (22.4% vs. 29.4%, Fig 1D), indicating that the subpopulation of dopaminergic neurons is not more or less sensitive to GDLS than the other neuronal cell types present. iPSCs were routinely characterized via standardized procedures (S1 Fig). To show GDLS can be widely implemented and is functional in the generation of different neuronal lineages, we applied the same approach to motor neurons differentiated from hiPS cells. This is illustrated in figure S2, where we show motor neurons can be successfully purified, and are electrically active using Ca^{2+} imaging.

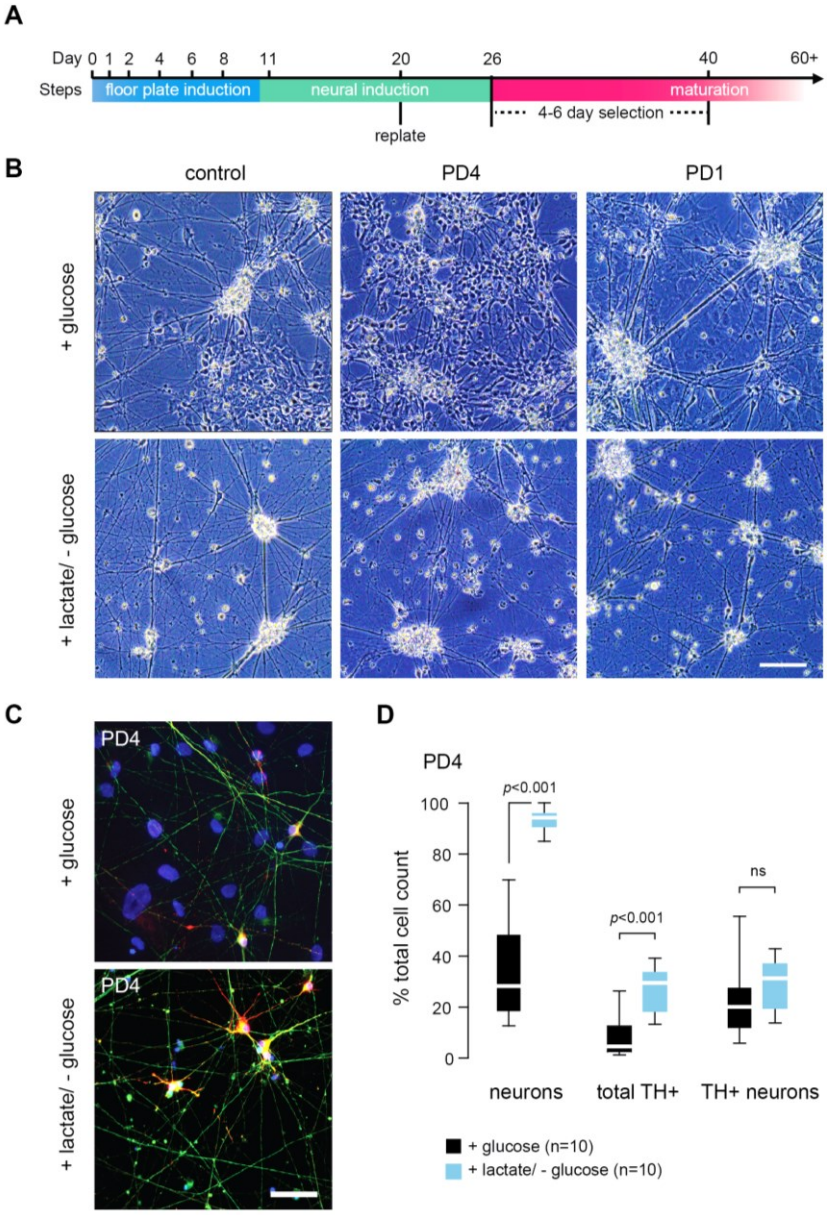

Figure 1. Glucose deprivation and lactate supplementation (GDLS) can be combined with dual SMAD inhibition. (A) *Schematic representation of the applied protocol for the differentiation and GDLS-treatment of hiPSCs.* ***(B)*** *Randomly selected phase contrast images of whole-well tile scan image of two*

PD patient lines and a control line. Selection was initiated at 30 DIV, and images were taken at 45 DIV (bars 100 µm). ***(C)*** *Fluorescent microscopy images for TUJ1 (green), TH (red) and Hoechst (blue) at 60DIV (bars 50 µm).* ***(D)*** *Quantifications of GDLS-treated (n=10) and control (n=10) cultures. Box plots (min to max) represent the percentage of neurons, percentage of TH-positive cells and percentage of TH-positive neurons.*

Purified neuronal cultures are electrophysiologically active

To assess the functional maturity of the neuronal cells obtained following GDLS, their electrical activity was measured at 60 DIV. Six days after GDLS treatment cells were replated on Geltrex® coated Labtek II chamber slides or coverslips. In addition, they were grown in BrainPhys™ medium plus growth factors for two weeks to electrically mature neuronal cells. Whole cell patch clamp recordings were performed on neurons derived from both control and PD1 patient iPS lines. Successful neuronal differentiation in patched samples was confirmed by subsequent staining for neuronal (TUJ1, red) and dopaminergic (TH, green) cells (Fig 2A).

A typical patch clamp recording experiment (current clamp mode) is depicted in Figure 2B, showing repetitive action potentials of both control (black) and PD1 patient-derived (blue) neurons. No differences were observed between GDLS-treated and -untreated neurons. Moreover, of 30 analyzed cells in three separate experiments in two iPS cell lines, all recorded cells were electrically active. Evoking repetitive action potentials with a 500 ms depolarizing current pulse resulted in an average of 5 spikes, with the amplitudes of the first spikes in a series averaging greater than 70 mV (Fig 2C). No differences in amplitudes of voltage-activated currents were observed between control (black) and PD1 patient (blue) iPSC neurons when recorded in voltage clamp mode (Fig 2D).

Calcium imaging experiments demonstrated that GDLS neurons display spontaneous firing activity, and are able to fire in synchrony (Fig 2E-G). Images containing multiple cells were analyzed over time as a

whole image, and individual cells were analyzed separately using a region of interest (ROI1/2, Fig 2E).

Neurons have the tendency to fire in synchrony, as evidenced by the same activity patterns in ROI1 and ROI2 (Fig 2G), and the overall trend observed in whole image analysis (Fig 2F). This indicates the formation of neuronal networks that are performing synchronous bursting, a hallmark of early neuronal plasticity (25, 26). Network activity patterns were observed in all recorded cultures, and showed synchronous bursting at rates of 2-3 field activations per minute, indicating neurons are able to electrically mature following GDLS treatment.

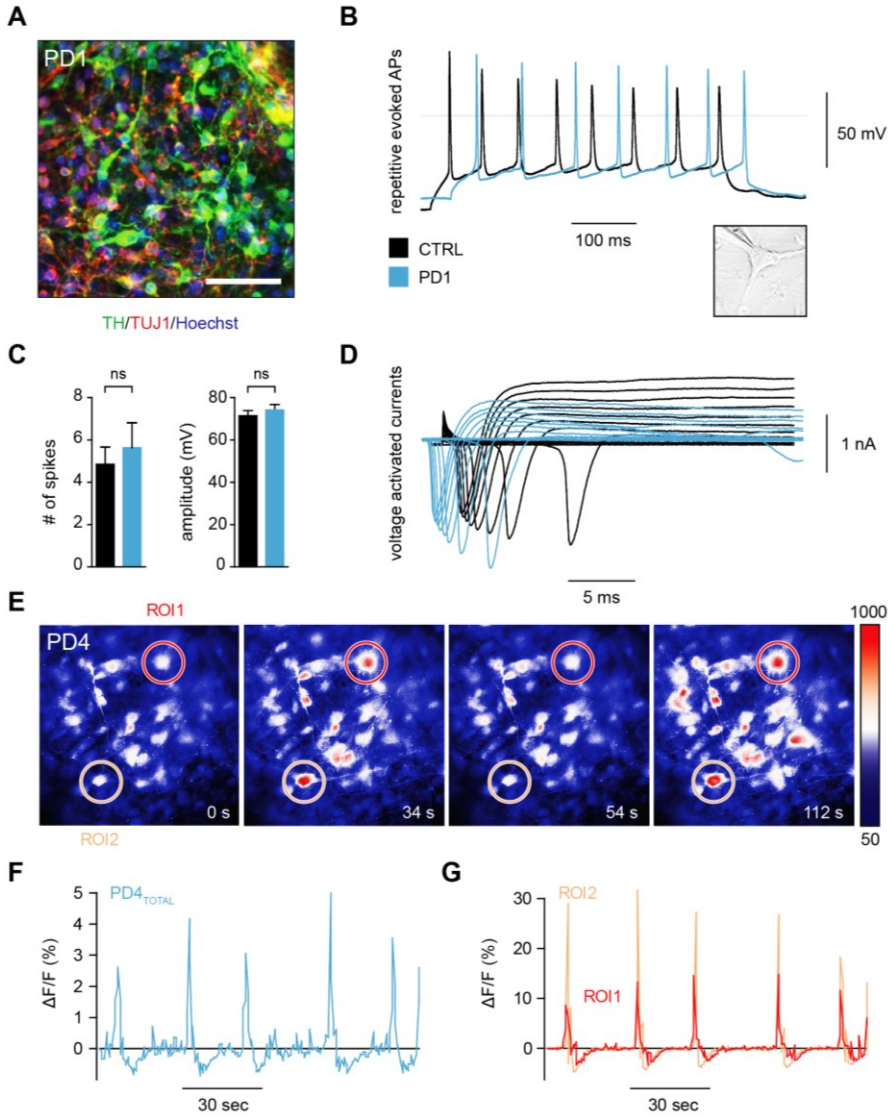

Figure 2. Neurons from patients and controls generate action potentials and perform synchronous bursting. ***(A)*** *Staining of patched samples at 60DIV using TH (green), TUJ1 (red) and Hoechst (blue) (bars 50 µm).* ***(B)*** *A representative repetitive evoked action potential recording of GDLS neurons.* ***(C)*** *Average spike amplitude was greater than 70 mV and neurons generated 5 action potentials on average. No differences were observed between neurons derived from patients and controls.* ***(D)*** *Representative voltage clamp recordings of GDLS*

*neurons in response to depolarizing voltage steps. In images **(B)**, **(C)** and **(D)** black represents a control line while blue represents a PD1 patient line. **(E)** Calcium imaging sequence of GDLS neurons showing spontaneous activity. **(F)** Calcium imaging analysis ($\Delta F/F_0$) of whole image and interspaced **(G)** neurons (ROI1/ROI2) demonstrates synchronous firing.*

GDLS-treated cultures have a greatly reduced astrocytic footprint and are enriched for the expression of neuronal marker genes

Since astrocytes are common contaminants in neuronal cultures derived from pluripotent stem cells we analyzed the occurrence of these cells in GDLS treated cultures. Immunocytochemical analysis of glial fibrillary acidic protein (GFAP) positive cells shows that GDLS treatment results in cultures that are almost completely devoid of astrocyte contamination (Fig 3A). Furthermore, the extent of the dopaminergic neuronal marker TH was not significantly altered upon GDLS treatment. Nuclear staining by Hoechst indicated a pronounced reduction in the total number of nuclei, suggesting that GDLS-treated cells have entered a post-mitotic phase and/or many non-neuronal cells have gone in apoptosis.

Total fluorescence was assessed in large tile scan stitches (n=5 per group) with a surface over 2.5 cm^2 (Fig 3C). An example of a complete tile scan stitch is presented in Figure 3B, showing both the size of the analyzed images and the homogenous cellular distribution, assuring that an imaging bias in the quantification is unlikely to occur.

GDLS results in a significant reduction in GFAP fluorescence, combined with a significant reduction in Hoechst fluorescence at all conditions (Fig 3C). TH content was not significantly altered between control and GDLS-treated conditions. An example of total fluorescence analysis is depicted in Figure S3.

In order to confirm the relative increase in neuronal cells in GDLS cultures, we determined mRNA expression levels of neuronal markers (Fig 3D). We observed enrichment for the general neuronal marker *TUJ1*. Expression of ventral midbrain dopaminergic markers *GIRK2*, *PITX3*, *OTX2* and *TH* also showed a robust enrichment when compared to untreated control

cells. Expression of the neuronal precursor and pluripotency marker *SOX2* shows reduced expression, indicating the loss of precursor cells and undifferentiated cells. In addition, the relative expression of the lactate transporter *MCT2* and lactate converting enzyme *LDHA* was increased. Summarizing, our data show the specific enrichment for neuronal populations after GDLS treatment, without having a deleterious effect on specific neuronal subtypes.

Inhibition of the MCT2 lactate transporter blocks selection

The brain lactate shuttle is thought to function through the MCT2 transporter protein (16). To confirm involvement of MCT2 and reveal the underlying mechanism of neuronal selection in our culture system, we used the MCT2 inhibitor alpha-cyano-4-hydroxycinnamic acid (4-CIN). Figure 4A shows a schematic overview of the experiment, wherein 100 µM of 4-CIN blocks the function of MCT2, while having a minor effect on the function of MCT1 and 4 (27).

Glucose-deprivation of cultures results in overall cell death, while GDLS-treated cells showed preferential survival of neuronal cells (Fig 4C-D). When 4-CIN was added during the GDLS procedure, cells were unable to take up lactate from the culture medium, leading to cell death at a similar rate as the glucose-deprived condition (Fig 4C-E). 4-CIN had no effect on cells supplemented with glucose, indicating that there was no direct toxic effect of 4-CIN (Fig 4B), while under GDLS conditions purification of neuronal populations was achieved (Fig 4D). Additional images of time courses of these experiments are presented in Figure S4, showing different time points of the experiment.

In summary, these data show that differentiated neuronal cells are capable of using lactate as a source of energy, in contrast to undifferentiated and glial cell types. Furthermore, these results confirm that the supplemented lactate is taken up through the MCT2 pathway.

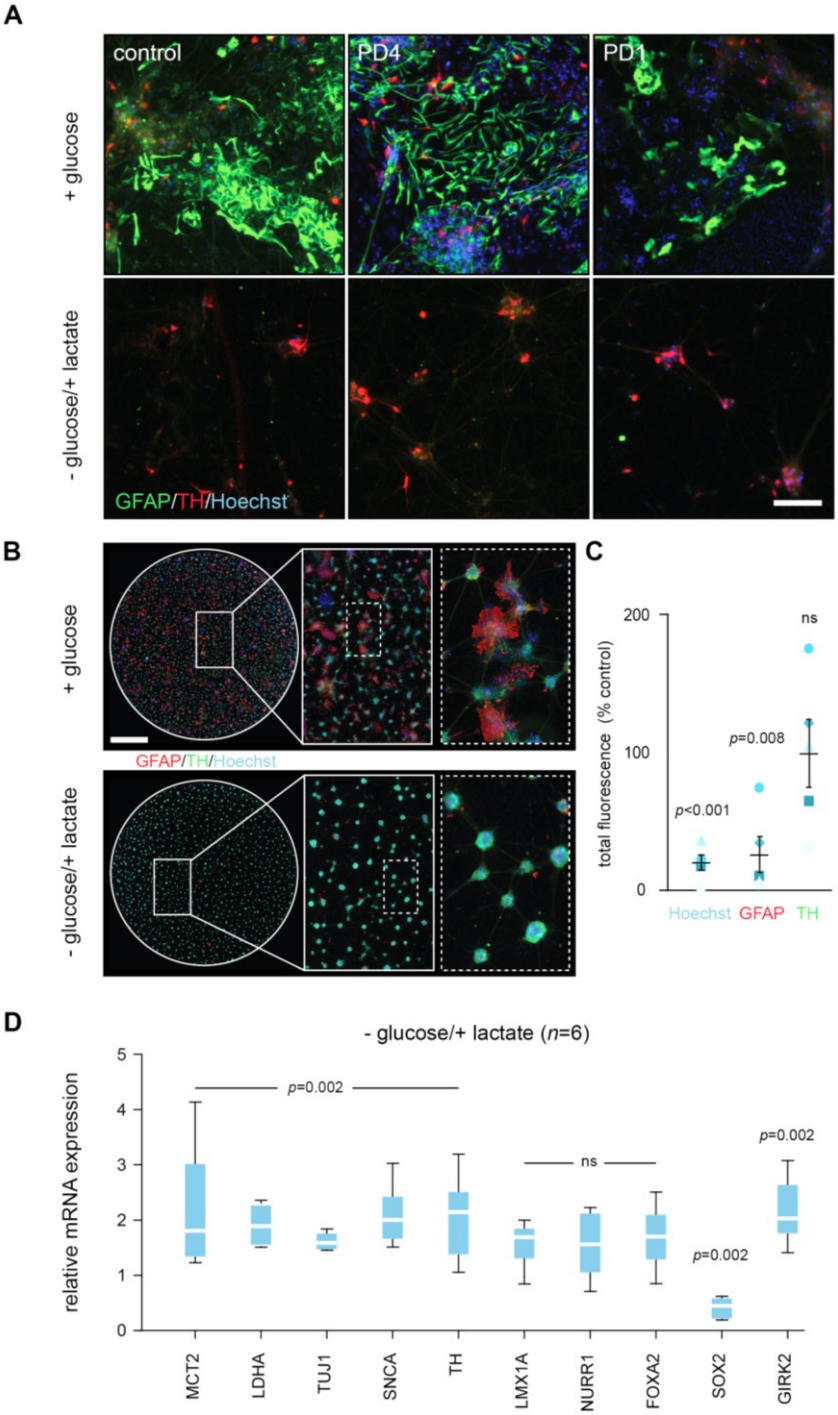
A
control
PD4
PD1
+ glucose
- glucose/+ lactate
GFAP/TH/Hoechst
B
+ glucose
- glucose/+ lactate
GFAP/TH/Hoechst
C
total fluorescence (% control)
200
100
0
ns
p=0.008
p<0.001
Hoechst
GFAP
TH
D
- glucose/+ lactate (n=6)
relative mRNA expression
5
4
3
2
1
0
p=0.002
ns
p=0.002
p=0.002
MCT2
LDHA
TUJ1
SNCA
TH
LMX1A
NURR1
FOXA2
SOX2
GIRK2

Figure 3. GDLS cultures demonstrate enrichment for neuronal markers and reduced expression of non-neuronal markers. (A) *Immunofluorescent images for Hoechst (blue), GFAP (green) and TH (red) of healthy and PD cell lines. Images are random excerpt of large scale tile scan stitches (>2,5 cm²) (bars 50 µm).* ***(B)*** *Large scale fluorescence surface analysis of Hoechst, GFAP, and TH (bars 200µm). Analysis was done using large tile scan images (>2,5 cm²), as depicted in* ***(C)****.* ***(D)*** *Expression analysis of neuronal and dopaminergic markers (TUJ1, SNCA, TH, LMX1A, NURR1 and GIRK2) in GDLS treated cultures, and the pluripotency and neuronal precursor marker SOX2. MCT2 and LDHA expression are upregulated in GDLS-treated cells. Non-treated cultures were used as reference value.*

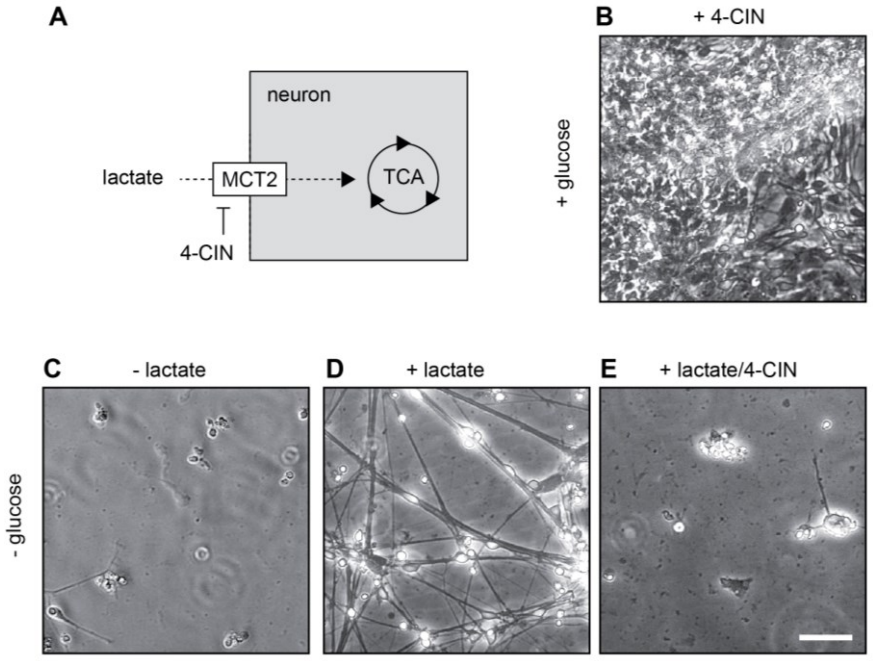

Figure 4. MCT-2 mediates GDLS neuronal selection. (A) *Schematic overview of the mechanism underlying 4-CIN inhibition.* ***(B-E)*** *Representative phase contrast images of control cells treated with glucose and 4-CIN* ***(B)*** *glucose and lactate deprivation* ***(C)*** *GDLS* ***(D)*** *and GDLS in combination with 4-CIN* ***(E)****.(bars 50 µm)*

Discussion and conclusion

The introduction of an effective, non-laborious and inexpensive protocol to purify hiPSC-derived neuronal cultures will provide the opportunity to perform complex experiments on these neurons, and use more pure cultures for disease modelling. Various protocols produce relatively pure neuronal cultures from human ESCs, but application of these protocols on hiPSCs often results in contamination with unwanted cell populations and proliferating cells. This hampers the use of long-term neuronal cultures, since contaminating proliferative cells will eventually overgrow neuronal cells. For this reason, many experiments are performed below 40 DIV (3), while more functional neurons arise around 60 DIV (28). At such early differentiation and maturation stages, late onset disease effects might not be measurable. Furthermore, early determination of differentiation efficiency lead to optimistic estimates of differentiation yields since proliferating cells progressively contaminate the neuronal cultures. While several articles have claimed high differentiation yields, it may prove difficult to replicate these results, due to subtle differences in culturing methods and the intrinsic variance in differentiation potential between iPSC lines (29).

Providing a cost-efficient and robust method to purify neuronal populations will make comparable high neuronal differentiation yields more accessible, and improve the outcome of many iPSC studies. Previously, cardiomyocytes have been purified from human ES cells by metabolic selection (30). Importantly, the selection approach efficiently used for pure cardiomyocytes, led to cell death in fetal mouse neuronal cells. Our results demonstrate that an adapted metabolic selection procedure on hiPSCs results in highly pure and viable neuronal cell cultures. These differences are likely attributable to media composition, since the absence of neurotrophic factors can lead to premature neuronal cell death.

We demonstrate that the GDLS selection procedure utilizes the MCT2 transporter and is based on the widely accepted concept of lactate

shuttling (14, 15, 17, 31). In this light, our data adds further evidence to the importance of lactate metabolism in neuroenergetics. This supports a view of lactate providing a beneficial effect, opposed to the classical view of lactate being associated with an allostatic load in the brain (31).
In summary, we have developed a method that makes the generation of pure neuronal cultures highly accessible. Importantly, GDLS does not negatively affect neuronal characteristics and greatly increases the relative amount of neuronal cells obtained from iPSC differentiation procedures.

Acknowledgements

We would like to thank Prof. Dr. Jon Laman for critical reading of the manuscript and Martijn Hoes from the Department of Experimental Cardiology (UMCG) for providing critical feedback during the experimental procedures.

References

1. Avior Y, Sagi I, Benvenisty N. Pluripotent stem cells in disease modelling and drug discovery. Nature reviews Molecular cell biology. 2016;17(3):170-82.
2. Goldman SA. Stem and Progenitor Cell-Based Therapy of the Central Nervous System: Hopes, Hype, and Wishful Thinking. Cell stem cell. 2016;18(2):174-88.
3. Torrent R, De Angelis Rigotti F, Dell'Era P, Memo M, Raya A, Consiglio A. Using iPS Cells toward the Understanding of Parkinson's Disease. Journal of clinical medicine. 2015;4(4):548-66.
4. Marx V. Stem cells: a dish of neurons. Nature methods. 2016;13(8):617-22.
5. Braak H, Del Tredici K, Rub U, de Vos RA, Jansen Steur EN, Braak E. Staging of brain pathology related to sporadic Parkinson's disease. Neurobiology of aging. 2003;24(2):197-211.
6. Freed CR, Breeze RE, Rosenberg NL, Schneck SA, Wells TH, Barrett JN, et al. Transplantation of human fetal dopamine cells for Parkinson's disease. Results at 1 year. Archives of neurology. 1990;47(5):505-12.

7. Woodard CM, Campos BA, Kuo SH, Nirenberg MJ, Nestor MW, Zimmer M, et al. iPSC-derived dopamine neurons reveal differences between monozygotic twins discordant for Parkinson's disease. Cell reports. 2014;9(4):1173-82.
8. Schondorf DC, Aureli M, McAllister FE, Hindley CJ, Mayer F, Schmid B, et al. iPSC-derived neurons from GBA1-associated Parkinson's disease patients show autophagic defects and impaired calcium homeostasis. Nature communications. 2014;5:4028.
9. Doi D, Samata B, Katsukawa M, Kikuchi T, Morizane A, Ono Y, et al. Isolation of human induced pluripotent stem cell-derived dopaminergic progenitors by cell sorting for successful transplantation. Stem cell reports. 2014;2(3):337-50.
10. Miller JD, Ganat YM, Kishinevsky S, Bowman RL, Liu B, Tu EY, et al. Human iPSC-based modeling of late-onset disease via progerin-induced aging. Cell stem cell. 2013;13(6):691-705.
11. Reinhardt P, Schmid B, Burbulla LF, Schondorf DC, Wagner L, Glatza M, et al. Genetic correction of a LRRK2 mutation in human iPSCs links parkinsonian neurodegeneration to ERK-dependent changes in gene expression. Cell stem cell. 2013;12(3):354-67.
12. Devine MJ, Ryten M, Vodicka P, Thomson AJ, Burdon T, Houlden H, et al. Parkinson's disease induced pluripotent stem cells with triplication of the alpha-synuclein locus. Nature communications. 2011;2:440.
13. Mazzulli JR, Xu YH, Sun Y, Knight AL, McLean PJ, Caldwell GA, et al. Gaucher disease glucocerebrosidase and alpha-synuclein form a bidirectional pathogenic loop in synucleinopathies. Cell. 2011;146(1):37-52.
14. Pellerin L, Magistretti PJ. Glutamate uptake into astrocytes stimulates aerobic glycolysis: a mechanism coupling neuronal activity to glucose utilization. Proceedings of the National Academy of Sciences of the United States of America. 1994;91(22):10625-9.
15. Machler P, Wyss MT, Elsayed M, Stobart J, Gutierrez R, von Faber-Castell A, et al. In Vivo Evidence for a Lactate Gradient from Astrocytes to Neurons. Cell metabolism. 2016;23(1):94-102.
16. Halestrap AP. The monocarboxylate transporter family--Structure and functional characterization. IUBMB life. 2012;64(1):1-9.
17. Hu Y, Wilson GS. A temporary local energy pool coupled to neuronal activity: fluctuations of extracellular lactate levels in rat brain monitored with rapid-response enzyme-based sensor. Journal of neurochemistry. 1997;69(4):1484-90.

18. Lee Y, Morrison BM, Li Y, Lengacher S, Farah MH, Hoffman PN, et al. Oligodendroglia metabolically support axons and contribute to neurodegeneration. Nature. 2012;487(7408):443-8.
19. Goyal MS, Hawrylycz M, Miller JA, Snyder AZ, Raichle ME. Aerobic glycolysis in the human brain is associated with development and neotenous gene expression. Cell metabolism. 2014;19(1):49-57.
20. Moussaieff A, Rouleau M, Kitsberg D, Cohen M, Levy G, Barasch D, et al. Glycolysis-mediated changes in acetyl-CoA and histone acetylation control the early differentiation of embryonic stem cells. Cell metabolism. 2015;21(3):392-402.
21. Kriks S, Shim JW, Piao J, Ganat YM, Wakeman DR, Xie Z, et al. Dopamine neurons derived from human ES cells efficiently engraft in animal models of Parkinson's disease. Nature. 2011;480(7378):547-51.
22. Chambers SM, Fasano CA, Papapetrou EP, Tomishima M, Sadelain M, Studer L. Highly efficient neural conversion of human ES and iPS cells by dual inhibition of SMAD signaling. Nature biotechnology. 2009;27(3):275-80.
23. Byers B, Cord B, Nguyen HN, Schule B, Fenno L, Lee PC, et al. SNCA triplication Parkinson's patient's iPSC-derived DA neurons accumulate alpha-synuclein and are susceptible to oxidative stress. PloS one. 2011;6(11):e26159.
24. Jiang H, Ren Y, Yuen EY, Zhong P, Ghaedi M, Hu Z, et al. Parkin controls dopamine utilization in human midbrain dopaminergic neurons derived from induced pluripotent stem cells. Nature communications. 2012;3:668.
25. Stephens CL, Toda H, Palmer TD, DeMarse TB, Ormerod BK. Adult neural progenitor cells reactivate superbursting in mature neural networks. Experimental neurology. 2012;234(1):20-30.
26. Wagenaar DA, Nadasdy Z, Potter SM. Persistent dynamic attractors in activity patterns of cultured neuronal networks. Physical review E, Statistical, nonlinear, and soft matter physics. 2006;73(5 Pt 1):051907.
27. Erlichman JS, Hewitt A, Damon TL, Hart M, Kurascz J, Li A, et al. Inhibition of monocarboxylate transporter 2 in the retrotrapezoid nucleus in rats: a test of the astrocyte-neuron lactate-shuttle hypothesis. The Journal of neuroscience : the official journal of the Society for Neuroscience. 2008;28(19):4888-96.
28. Pre D, Nestor MW, Sproul AA, Jacob S, Koppensteiner P, Chinchalongporn V, et al. A time course analysis of the electrophysiological properties of neurons differentiated from human induced pluripotent stem cells (iPSCs). PloS one. 2014;9(7):e103418.

29. Hu BY, Weick JP, Yu J, Ma LX, Zhang XQ, Thomson JA, et al. Neural differentiation of human induced pluripotent stem cells follows developmental principles but with variable potency. Proceedings of the National Academy of Sciences of the United States of America. 2010;107(9):4335-40.
30. Tohyama S, Hattori F, Sano M, Hishiki T, Nagahata Y, Matsuura T, et al. Distinct metabolic flow enables large-scale purification of mouse and human pluripotent stem cell-derived cardiomyocytes. Cell stem cell. 2013;12(1):127-37.
31. Mason S. Lactate Shuttles in Neuroenergetics-Homeostasis, Allostasis and Beyond. Frontiers in neuroscience. 2017;11:43.

Supplemental figures

S1 Fig.pdf vZomeren et al, 2017

Figure S1. Characterization of iPSC lines, related to Figure 1
(A) Phase contrast image of feeder free iPSC culture. (B) iPSC culture stained with Live Alkaline Phosphatase staining (Thermo Scientific). (C) Embryoid body formation. (D-F) iPSC immunocytochemistry for various pluripotency markers. (D) Staining for OCT4 (green), SOX2 (red) and Hoechst (blue). (E) Staining for NANOG (green), SSEA4 (red) and Hoechst (blue) (F) Staining for TRA1-81 (red) and Hoechst (blue) (G-I) Embryoid body immunocytochemistry for DESMIN (red) and Hoechst (blue) (G), TUJ1 (green) and Hoechst (blue) (I) and GATA4 (red) and Hoechst (blue) (J). Scalebar is 50μm

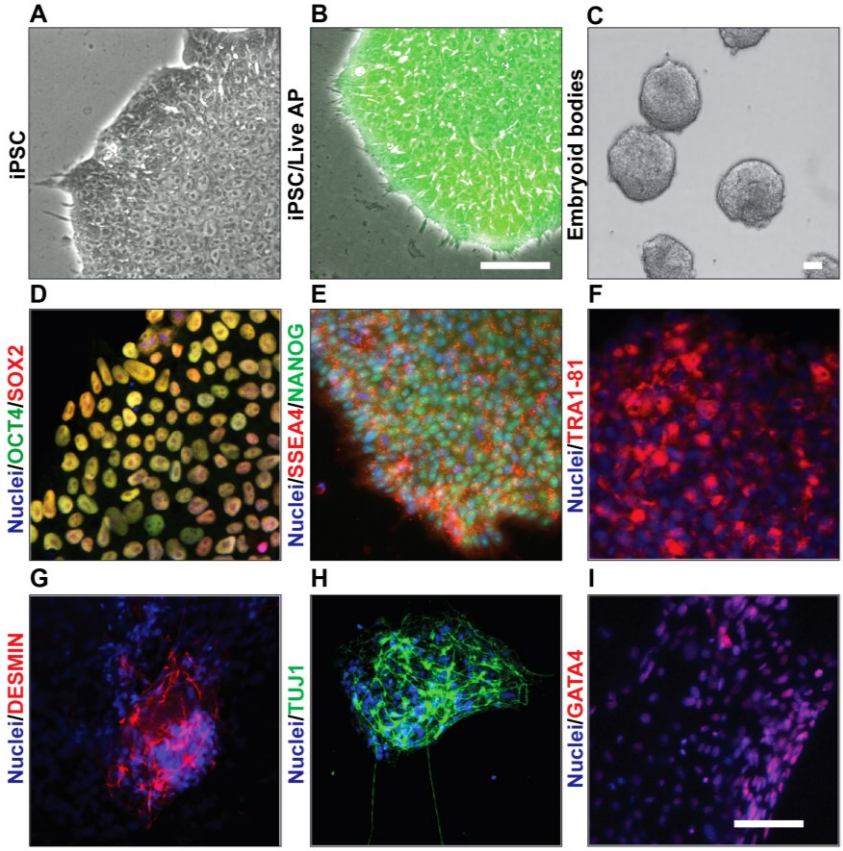

S2 Fig.pdf vZomeren et al, 2017

Figure S2. Motor neuron (MN) differentiation based on dual SMAD inhibition, related to Figure 1. (A) Applied protocol for the differentiation of MN and GDLS-treatment of hiPSCs. (B) Non-treated and GDLS treated MN cultures at 30DIV. (C) Staining of MN at 45DIV using ChAT (green), TUJ1 (red) and Hoechst (blue). (D) MN cultures incubated with 0.5 µM Fluo-AM at 45DIV (E) Calcium imaging analysis (ΔF/F0) of whole image. (F) Corresponding images to time points 20s, 47s, 81s and 82s in calcium imaging analysis. All experiments were performed with a control iPSC line Scalebar represents 100µm in all images.

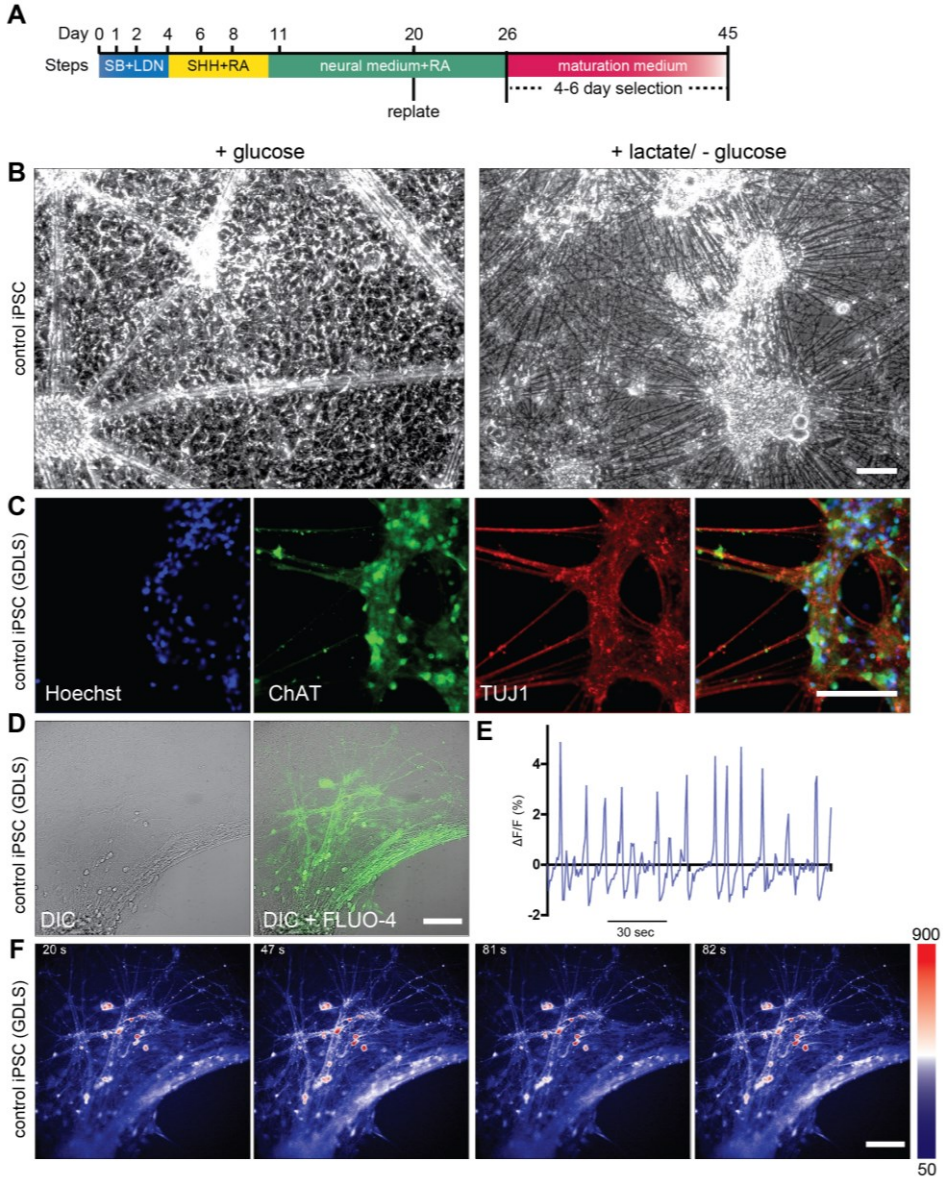

S3 Fig.pdf vZomeren et al, 2017

Figure S3. Analysis of immunofluorescent surface, related to Figure 3
Fluorescent images show an example of the assessment of fluorescence surface analysis for Hoechst (blue), GFAP (red) and TH (green) in both control and GDLS treated condition. Similar thresholding was used, and black and white images used for quantification are shown. Total surface of these analysis image was >6 cm2.

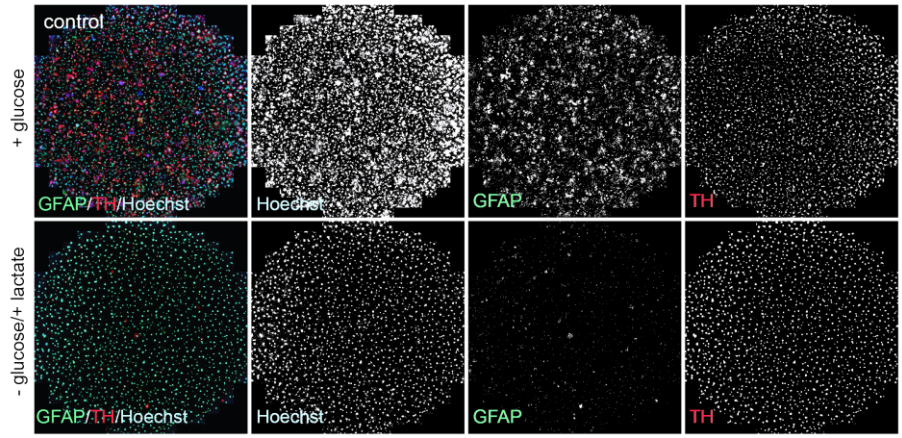

S4 Fig.pdf vZomeren et al, 2017

Figure S4. MCT2 inhibition over different time points, related to Figure 4
In a time dependent series of Figure 4, cells are followed over a period of 4 days, with a glucose (25mM) recovery phase at day 5 and 6. (A) Illustrates glucose (25mM) containing medium supplemented with 100 µM 4-CIN. (B) Shows glucose deprived cells without additional lactate supplementation. (C) GDLS treated cultures show preferential survival of neuronal cells, which is blocked if 4-CIN is added to the medium (D).